Transactions of the Korean Nuclear Society Autumn Meeting
Gyeongju, Korea, October 29-30, 2026

Homogeneous (Th,U)O_2 Fuel for a Long Single-Batch Cycle in a NuScale-like SMR Core

Rafał Dziedzic and Yoon Joo-il*
Department of Nuclear Power Plant Engineering, KEPCO International Nuclear Graduate School (KINGS)
**Corresponding author: jiyoon@kings.ac.kr*

***Keywords : Radial fuel zoning, Loading pattern, Power peaking, Boron-free core, Two-step neutronics**

1. Introduction

Small modular reactors (SMRs) are the subject of broad international design activity: a recent review identified 141 designs worldwide, approximately 55% of them at technology readiness level 1 [1], indicating that much of the design space remains at a very early maturity stage. Most concepts are therefore still at a stage at which the core and its fuel remain open design problems. Long refuelling intervals are among the deployment features attributed to these reactors, together with electricity and process heat for remote or off-grid communities, mining, and industry [2]. Carried to its limit, such an interval gives a single-batch core, loaded once and operated until discharge, for which the governing design quantity is the burnup reached before k_{eff} falls to unity. The fuel composition is the lever used here. Thorium is the more abundant element, with a present-day theoretical thorium-to-uranium ratio of approximately 3.9 against a lithospheric average of 3–4 [3]. In a ThO_2–UO_2 core its fraction can be varied in magnitude and in space, which makes it a single lever acting on the reactivity trajectory and on the radial power shape at once. Both constrain the design: the all-fresh, boron-free core modelled here holds its excess reactivity from the beginning of life, and the radial power distribution bounds how far the composition can be driven. The present study therefore treats fuel and core as one design problem for a NuScale-like SMR. Its scope covers homogeneous ThO_2–UO_2 compositions, systematic composition sweeps, and full-core loading patterns, examined for their coupled effects on criticality evolution and spatial power over the cycle, and it identifies configurations meeting the project-defined cycle-length and power-distribution criteria.

2. Computational Methodology

2.1. Design objectives and fixed model conditions

A literature review established the performance context, after which the authors adopted the screening objectives in Table I.

The two peaking metrics were calculated from axially integrated powers as

$$\text{PPF} = \frac{P_{\text{FA,max}}}{\overline{P}_{\text{FA}}}, \qquad F_r = \frac{P_{\text{pin,max}}}{\overline{P}_{\text{pin}}}. \tag{1}$$

Table I Screening objectives.

Metric	Definition	Target
Critical burnup	$k_{\text{eff}} = 1$ crossing	> 50 GWd/tHM
Full-power days	EFPD at the crossing	> 2800 d
PPF	peak/mean assembly power	< 1.40
F_r	peak/mean pin power	< 1.45

The overbars denote core-wide means over the 37 assemblies or all fuel pins, and the maximum values over depletion were used. Critical burnup and EFPD were obtained by linear interpolation at the $k_{\text{eff}} = 1$ crossing. The BOL eigenvalue reported below is the full-core SPHINCS k_{eff} at zero burnup under the conditions of Table II, and the corresponding excess reactivity is $\rho = (k_{\text{eff}} - 1)/k_{\text{eff}}$. The all-fresh model represents a single-batch cycle, not equilibrium discharge burnup. The conditions held fixed across every calculation are listed in Table II.

Table II Fixed model conditions adapted from the benchmark [4].

Parameter	Value or condition
Power / active height	160 MW_{th} / 200 cm
Core / assembly	37 fresh FAs, one batch / 17×17
Fuel / moderator temperature	900 K / 600 K
Boron / burnable absorbers	0 ppm / none
Thermal feedback	disabled
Depletion range	0–60 GWd/tHM

2.2. Fuel architecture and sequential design space

Preliminary seed–blanket arrangements were screened before adopting a homogeneous 17×17 lattice with 264 identical fuel pins, 24 guide tubes, and one instrumentation tube. Every homogeneous composition contains exactly 20.00 wt% U-235 in uranium [8]. THWx denotes x wt% ThO_2 and $(100 - x)$ wt% UO_2. Only this oxide split varies, from THW50 to THW95. Fuel density follows the project 96% TD ideal specific-volume approximation. These compositions were distributed over the core through the project-defined EOCS pattern, which contains 16 peripheral A01, 12 B01, eight C01, and one central D01 assembly (Fig. 1). Nine batches varied the ThO_2 content and radial gradient in three sequential stages (Table III), giving 54 full-core depletion cases. Stages II and III were selected after reviewing the preceding stage. A case qualified only if all four objectives in Table I were met simultaneously. The assembly-count-weighted core-

average ThO_2 content was calculated as

$$\overline{w}_{ThO_2} = \frac{16w_A + 12w_B + 8w_C + w_D}{37}, \qquad (2)$$

where w_A–w_D are the ThO_2 contents of the corresponding assembly types in wt%.

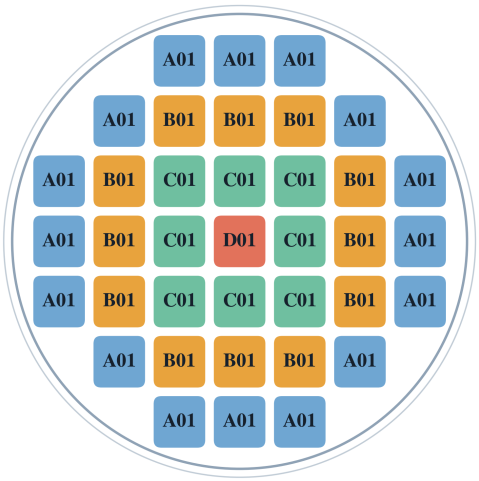


Fig. 1. Project-defined EOCS loading pattern; A01 is the peripheral assembly type and D01 the central one.

Table III Sequential fuel-design space; six cases per batch.

Batch	Anchor [wt% ThO_2]	Δ [wt%]	$\overline{w}_{ThO_2}$ [wt%]
B1	D01 = 90–95	1	87.84–92.84
B2	D01 = 90–95	5	79.19–84.19
B3	D01 = 90–95	10	68.38–73.38
B4	A01 = 60–65	2	61.68–66.68
B5	A01 = 60–65	4	63.35–68.35
B6	A01 = 60–65	8	66.70–71.70
B7	A01 = 50–55	5	54.19–59.19
B8	A01 = 50–55	8	56.70–61.70
B9	A01 = 50–55	11	59.22–64.22

2.3. Reference core, code system, and data generation

The geometry follows the 37-assembly NuScale-like benchmark of Fridman et al. [4]. DeCART2D is two-dimensional and cannot reproduce that three-dimensional core on its own, so the geometry model was verified with the Monte Carlo code PRAGMA, and the two-step chain by passing PRAGMA-homogenized cross sections to SPHINCS. The reference calculation compared k_{eff} and the axial, assembly, and pin-power distributions with the published solution. Table IV lists the three solutions at the benchmark reference state, which uses 1000 ppm boron, fully withdrawn rods, and ENDF/B-VII.1 data. Agreement with the benchmark reference solution demonstrates consistency of the code chain at that state. It does not reflect the boron-free thorium variants screened below, which carry their own libraries; that model is a design variant of the benchmark, not its literal reproduction. The design workflow then generated its own data. Each homogeneous composition was depleted in a reflective single-assembly DeCART2D model from 0 to 60 GWd/tHM at the conditions of Table II [5], and the resulting burnup-dependent libraries were mapped to the A01–D01 SPHINCS fuel sets. Reflector data were homogenized with PRAGMA [7], and SPHINCS carried the three-dimensional full-core depletion and power calculation [6]. Finally, for a controlled comparison, B8/A52 was also depleted with an UO_2-only fuel set adjusted to reproduce the same initial whole-core U-235 inventory; all other core and depletion conditions were unchanged.

Table IV Reference-state verification; Monte Carlo standard deviations on the last digits in parentheses.

Solution	Method	k_{eff}
Serpent [4]	continuous-energy Monte Carlo	1.02768(1)
PRAGMA	continuous-energy Monte Carlo	1.027278(32)
SPHINCS	pin-wise diffusion, homogenized	1.028107

3. Results and Discussion

3.1. Sequential screening and final design space

Batches B1–B3 explored ThO_2-rich cores. B1 was subcritical from BOL, whereas B2 and B3 reached critical burnups of 2.7–16.8 and 26.7–35.9 GWd/tHM. Batches B4–B6 lowered the core-average ThO_2 content and exposed the central trade-off. Shallow gradients preserved burnup but raised radial peaking, whereas steeper gradients flattened the power distribution at the expense of burnup. None met all four objectives simultaneously. The final B7–B9 stage examined 18 lower-anchor designs. All B7 cases exceeded 50 GWd/tHM but failed the F_r objective. Increasing the gradient in B8 and B9 reduced both peaking metrics, while the associated increase in $\overline{w}_{ThO_2}$ shortened the cycle. Four retained designs met all screening objectives. Figures 2 and 3 summarize this stage.

3.2. Designs meeting the screening objectives

Table V lists the four composition-matched designs retained after applying all objectives simultaneously.

Table V Retained designs satisfying all screening objectives; the second column is the ThO_2 content of the A01, B01, C01 and D01 assembly types, from the core periphery inwards.

Core	A01/B01/ C01/D01 [wt%]	$\overline{w}_{ThO_2}$ [wt%]	burnup [GWd/tHM]	EFPD [d]	PPF	F_r	k_{eff} BOL
B9/A50	50/61/72/83	59.2	50.74	2808	1.225	1.380	1.3070
B8/A53	53/61/69/77	59.7	50.68	2803	1.266	1.404	1.3135
B8/A52	52/60/68/76	58.7	52.24	2892	1.278	1.406	1.3188
B8/A50	50/58/66/74	56.7	55.29	3067	1.300	1.422	1.3288

B9/A50 has the flattest power distribution but only 0.74 GWd/tHM of critical-burnup margin, B8/A50 the largest burnup margin at the highest peaking, and B8/A52 lies between them. All four begin at $k_{eff} = 1.3070$–1.3288, an excess reactivity of 23,488–24,746 pcm left uncompensated in the present boron-free model. The representative B8/A52 BOL map in Fig. 4 has a maximum assembly power of 1.278 and a minimum of 0.694. Figure 5 shows the full depletion trajectories of the four retained designs. Their ordering persists throughout burnup, with B8/A50 remaining the most reactive and B9/A50 and B8/A53 reaching $k_{eff} = 1$ first.

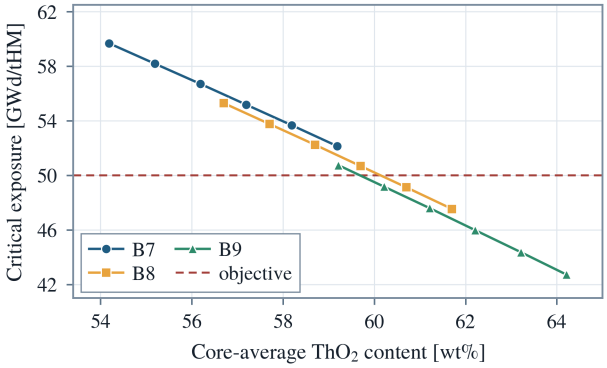


Fig. 2. Critical burnup for the B7–B9 stage; the dashed line is the 50 GWd/tHM objective.

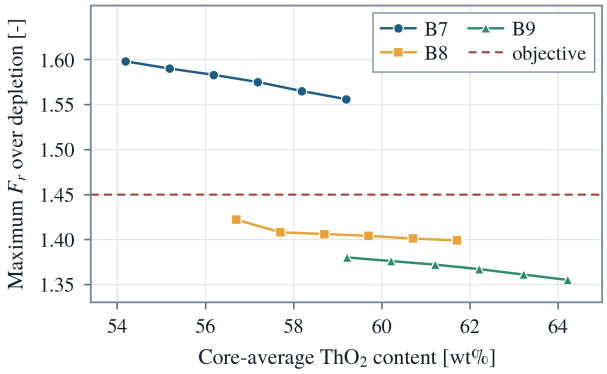


Fig. 3. Maximum F_r over depletion for the B7–B9 stage; the dashed line is the $F_r = 1.45$ objective.

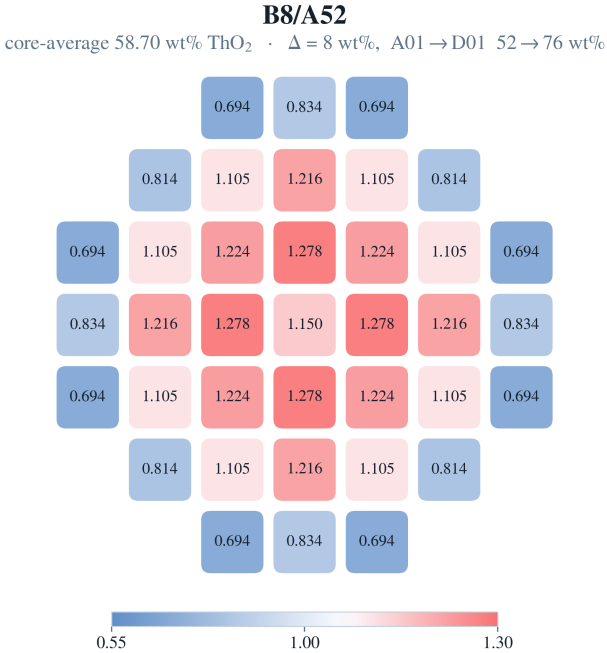


Fig. 4. Representative B8/A52 BOL assembly-power distribution, normalized to the core mean; maximum 1.278, minimum 0.694.

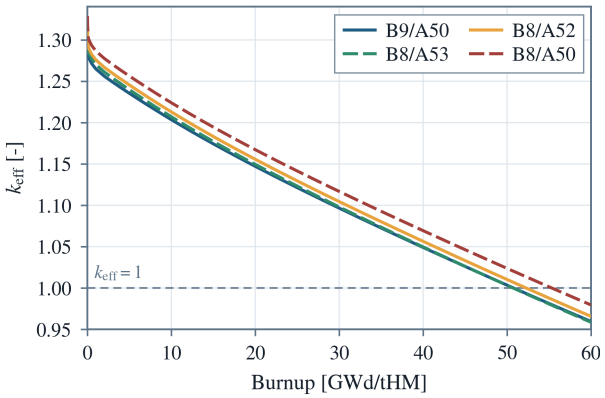


Fig. 5. Full-core k_{eff} evolution of the four retained configurations; the dashed line denotes $k_{eff} = 1$.

3.3. Iso-fissile UO_2 reference comparison

B8/A52 was selected for the controlled comparison. Table VI confirms essentially identical initial U-235 inventories, while the different fertile matrices produce different total heavy-metal inventories.

Table VI Initial heavy-metal inventories for B8/A52 and the UO_2 reference.

Inventory	B8/A52 [kg]	UO_2 ref. [kg]
Th-232	5189.73	0.00
U-235	733.49	733.52
U-238	2933.97	8639.66
Total HM	8857.19	9373.18

Despite the matched U-235 inventory, the UO_2 reference starts at a higher k_{eff} but decreases more rapidly with burnup (Fig. 6). The difference at the beginning of life is 9,734 pcm in k_{eff}, 1.31884 against 1.41618. The interpolated critical burnups are 52.24 and 51.65 GWd/tHM for B8/A52 and the UO_2 reference, respectively. Their corresponding crossing times are 2892 and 3026 EFPD because the UO_2 reference contains more heavy metal.

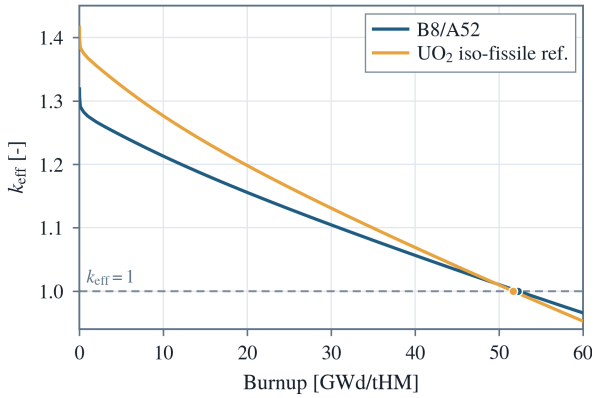


Fig. 6. k_{eff} evolution of B8/A52 and the UO_2-only iso-fissile reference; the markers are the interpolated critical crossings.

The isotopic evolution in Fig. 7 shows the different fertile-to-fissile pathways directly: B8/A52 progressively develops U-233 and holds 2.28 kg of Pa-233 at its critical crossing, whereas the UO_2 reference develops a larger Pu-239 inventory, 61.6 against 28.9 kg. This behavior

is consistent with the different reactivity trajectories and shows that the comparison cannot be reduced to the initial U-235 loading alone.

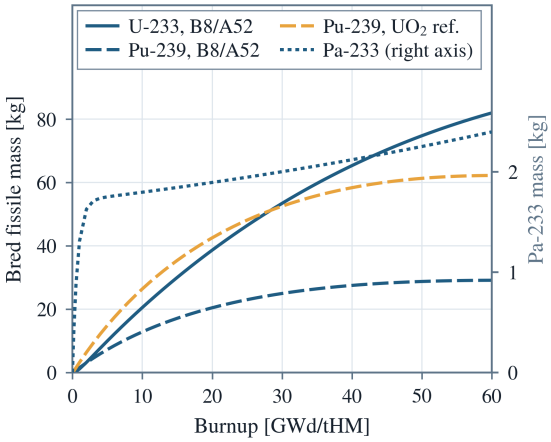


Fig. 7. Whole-core bred inventories; the colour denotes the case and the dash pattern the nuclide, with the Pa-233 holdup of B8/A52 read on the right-hand axis.

4. Conclusions

This study developed a fuel-and-loading-pattern design pathway for a homogeneous ThO_2–UO_2 NuScale-like SMR core targeting long single-batch operation while maintaining the adopted power-distribution limits. Nine sequential batches comprising 54 full-core depletion cases revealed a clear trade-off: shallower ThO_2 gradients preserve critical burnup but increase radial power peaking, whereas stronger gradients flatten the power distribution at the cost of cycle length. Four EOCS configurations were identified that satisfy all four screening objectives simultaneously, achieving 50.68–55.29 GWd/tHM, 2803–3067 EFPD, PPF of 1.225–1.300, and F_r of 1.380–1.422. The study therefore defines not only a single feasible solution, but a retained design region in which long-cycle performance and radial power control can be balanced through fuel zoning. The controlled iso-fissile comparison further showed that B8/A52 reaches a critical burnup of 52.24 GWd/tHM compared with 51.65 GWd/tHM for the UO2 reference, despite starting 9,734 pcm lower in *k*eff. It also develops the U-233 production pathway and accumulates 28.9 kg of Pu-239 by the critical crossing, compared with 61.6 kg for the UO_2 core. These results show that the observed long-cycle behavior is not determined by initial U-235 loading alone, but also by the different fertile matrix and its isotopic evolution. The remaining limitation is reactivity control: the retained boron-free configurations contain 23,488–24,746 pcm of uncompensated BOL excess reactivity. Further work will therefore introduce burnable absorbers to control this excess while preserving the established cycle-length and PPF/F_r margins. BeO corner reflectors are also considered as a means of improving neutron economy and assessing reflector effects in the thorium-bearing core.

Acknowledgment

This research was supported by the 2026 Research Fund of the KEPCO International Nuclear Graduate School (KINGS), the Republic of Korea.

REFERENCES

[1] J.S. Kang, I.G. Chang, and J.H. Cheong, “Comprehensive review of small modular reactor development focusing on challenges in the backend nuclear fuel cycle,” *Nuclear Engineering and Technology*, vol. 58, 104000, 2026.
[2] D. Michaelson and J. Jiang, “Review of integration of small modular reactors in renewable energy microgrids,” *Renewable and Sustainable Energy Reviews*, vol. 152, 111638, 2021.
[3] C. Degueldre and M.J. Joyce, “Evidence and uncertainty for uranium and thorium abundance: A review,” *Progress in Nuclear Energy*, vol. 124, 103299, 2020.
[4] E. Fridman, Y. Bilodid, and V. Valtavirta, “Definition of the neutronics benchmark of the NuScale-like core,” *Nuclear Engineering and Technology*, vol. 55, pp. 3639–3647, 2023.
[5] A. Dandi and M.H. Kim, “Conceptual design of the double tube burnable poison for the next generation small modular reactor,” *Annals of Nuclear Energy*, vol. 186, 109776, 2023.
[6] D.P. Szymczyna and J. Yoon, “Transient analysis of the SPERT III E-core experiment with nTRACER/SPHINCS code system,” *Nuclear Engineering and Technology*, vol. 58, 104011, 2026.
[7] J. Kim, S.Y. Hwang, T.S. Jung, and J. Yoon, “Optimization of spent fuel reduction and reactivity control using LEU+ fuel and hybrid burnable absorbers in innovative small modular reactors,” *Nuclear Engineering and Technology*, vol. 58, 104059, 2026.
[8] G. Laranjo de Stefani et al., “Particle swarm optimization of a small modular reactor fuel assembly design with composed of U–Zr plates and MOX pins, based on Radkowsky concept,” *Progress in Nuclear Energy*, vol. 191, 106058, 2026.